

Article

All-Dielectric Metasurface for Sensing Microcystin-LR

Binze Ma ¹, Ao Ouyang ¹, Juechen Zhong ¹, Pavel A. Belov ², Ravindra Kumar Sinha ^{3,4}, Weiping Qian ⁵, Pintu Ghosh ^{1,*} and Qiang Li ^{1,*}

- ¹ State Key Laboratory of Modern Optical Instrumentation, College of Optical Science and Engineering, Zhejiang University, Hangzhou 310027, China; binzem@zju.edu.cn (B.M.); 21830006@zju.edu.cn (A.O.); 21830021@zju.edu.cn (J.Z.)
- ² Department of Physics and Engineering, ITMO University, Saint Petersburg 197101, Russia; belov@metalab.ifmo.ru
- ³ TIFAC-CORE in Fiber Optics and Optical Communication, Applied Physics Department, Delhi Technological University, Bawana Road, Delhi 110042, India; dr_rk_sinha@yahoo.com
- ⁴ CSIR-Central Scientific Instruments Organization, Chandigarh 160030, India
- ⁵ State Key Laboratory of Bioelectronics, Southeast University, Nanjing 210096, China; wqian@seu.edu.cn
- * Correspondence: ghosh@zju.edu.cn (P.G.); qiangli@zju.edu.cn (Q.L.)

Abstract: Sensing Microcystin-LR (MC-LR) is an important issue for environmental monitoring, as the MC-LR is a common toxic pollutant found in freshwater bodies. The demand for sensitive detection method of MC-LR at low concentrations can be addressed by metasurface-based sensors, which are feasible and highly efficient. Here, we demonstrate an all-dielectric metasurface for sensing MC-LR. Its working principle is based on quasi-bound states in the continuum mode (QBIC), and it manifests a high-quality factor and high sensitivity. The dielectric metasurface can detect a small change in the refractive index of the surrounding environment with a quality factor of ~ 170 and a sensitivity of ~ 788 nm/RIU. MC-LR can be specifically identified in mixed water with a concentration limit of as low as 0.002 $\mu\text{g/L}$ by a specific recognition technique for combined antigen and antibody. Furthermore, the demonstrated detection of MC-LR can be extended to the identification and monitoring of other analytes, such as viruses, and the designed dielectric metasurface can serve as a monitor platform with high sensitivity and high specific recognition capability.

Keywords: all-dielectric metasurface; quasi bound states in the continuum; microcystin-LR; specific recognition; high sensitivity



Citation: Ma, B.; Ouyang, A.; Zhong, J.; Belov, P.A.; Sinha, R.K.; Qian, W.; Ghosh, P.; Li, Q. All-Dielectric Metasurface for Sensing Microcystin-LR. *Electronics* **2021**, *10*, 1363. <https://doi.org/10.3390/electronics10111363>

Academic Editor: Ganapathy Senthil Murugan

Received: 7 May 2021

Accepted: 5 June 2021

Published: 7 June 2021

Publisher's Note: MDPI stays neutral with regard to jurisdictional claims in published maps and institutional affiliations.



Copyright: © 2021 by the authors. Licensee MDPI, Basel, Switzerland. This article is an open access article distributed under the terms and conditions of the Creative Commons Attribution (CC BY) license (<https://creativecommons.org/licenses/by/4.0/>).

1. Introduction

Microcystin is a kind of biotoxin widely found in freshwater bodies across the world [1–4]. It is one of the indicators of water eutrophication which makes water consumption harmful to human beings [5–8]. Microcystin can inhibit the production of protein phosphatase in cells and exposure to microcystin can severely damage organs, including liver, intestines, lungs, and kidneys [5–12]. There are many variants of microcystin, such as MC-LR, MC-RR, and MC-YR (L, R, and Y stand for leucine, arginine, and tyrosine, respectively). Among them, MC-LR is the most common and the most toxic variant [5,6,13]. According to the World Health Organization recommendations, the MC-LR content in drinking water shall not exceed 1 $\mu\text{g/L}$ [14]. In order to effectively manage microcystin and reduce its health risks, there is an urgent need for a sensitive and reliable method to detect microcystin, especially MC-LR.

Traditionally, the detection of MC-LR relies on an enzyme-based biochemical or chemical chromatography method, and it involves a trade-off between sensitivity and response speed [15–19]. In this regard, metasurface-based sensors can provide a feasible solution with their high sensitivity, real-time analysis, and label-free process [20–22]. The metasurface is ultrathin metamaterials consisting of planar microstructures (e.g., meta-atoms) with pre-determined electromagnetic responses arranged in specific sequences,

and it enables strong interactions with the electric and/or magnetic components of the incident electromagnetic fields [21–27]. Due to strong enhancement of the electric field, metasurface based on surface plasmon resonances (SPR metasurface) using metal can detect the presence of MC-LR even at very low concentrations. Hu et al. introduced an indirect SPR immune sensor by covalently linking the coupling of bovine serum albumin and microcystin to the carboxymethyl dextran on the gold surface of a sensor chip [20]. Sonia Herranz et al. systematically evaluated the performance of an SPR biosensor with a sensitivity of 0.2 $\mu\text{g}/\text{L}$ [21]. In addition to sensitivity, the quality factor is also used to evaluate the performance of metasurface-based sensors [21,24,25]. The quality factor is defined as the underdamped condition of resonance [24,25]. Although the SPR metasurface provides a highly sensitive detection strategy for MC-LR, the quality factor is limited by the intrinsic loss of metal, and the thermal effect of metal inevitably damages the living tissues in case of an in vivo sensing [26–29].

Dielectric metasurface with high-refractive index and low intrinsic loss has the potential to overcome these limitations [30–47]. Compared with an SPR metasurface, a dielectric metasurface has three distinct advantages. Firstly, a dielectric metasurface can achieve a higher quality factor compared to an SPR metasurface due to its low intrinsic loss [31–34]. Secondly, dielectric such as silicon is harmless to biomolecules without the thermal effect, and thereby, the dielectric metasurface can work for in vivo sensing [35,36]. Finally, the dielectric metasurface supports not only electric resonance mode but also magnetic resonance mode and higher-order multipole modes [37–47]. Therefore, dielectric metasurfaces are expected to provide new directions and technologies for label-free detection of MC-LR owing to its high-quality factor and high sensitivity.

In this article, we demonstrate an all-dielectric metasurface based on periodic arrays of elliptical silicon disc pairs for sensing MC-LR with high-quality factor and high sensitivity. These elliptical silicon disc pairs support quasi-bound states in the continuum mode (QBIC), which, in turn, supports resonance with narrow linewidth and strong electric field enhancement in the near-field region of QBIC. Based on this technique, small changes in the refractive index of enhancement region can be detected by the dielectric metasurface with a quality factor of ~ 170 and a sensitivity of ~ 788 nm/RIU (refractive index unit). In addition, combined with the antigen-antibody binding technique, the dielectric metasurface realizes the specific recognition of MC-LR even at low concentrations. The limiting concentration for sensing MC-LR in the experiment turns out to be as low as 0.002 $\mu\text{g}/\text{L}$.

2. Materials and Methods

2.1. Numerical Simulation

The metasurface was designed using three-dimensional Finite-Difference Time-Domain (FDTD) solutions. The refractive index of silicon and silica were taken from the inbuilt database in FDTD [48]. A normal-incident plane wave source was considered while calculating the transmission and reflection properties of the dielectric metasurface. A mesh size of 10 nm was set over the whole volume of the elliptical silicon disc pair. The top and bottom boundaries were set as perfectly matched layers to suppress the reflections from the boundaries. The side boundaries were set as period layers for simulation of the periodic arrays.

2.2. Fabrication

The metasurface was fabricated on a silicon on insulator (SOI) substrate. A 200 nm-thick negative resist (AR-N 7520.11) was spun coated onto the SOI substrate and baked on a hotplate for 1 min at 85 °C. Thereafter, the resist was exposed to electron beam lithography (RAITH VOYAGER) to define the structure pattern. Next, it was developed in AR300-47 for 50 s and rinsed in deionized water for 30 s. The residual resist acts like a mask to resist etching during the reactive ion etching process (OXFORD PlasmaPro 100 Cobra 180) to transfer the designed pattern to the layer below. The arrays of elliptical silicon disc pairs were finally prepared after oxygen plasma cleaning.

2.3. Refractive Index Sensing

Glucose solutions with different mass fractions were dropped on the surface of the metasurface, and the amount of each droplet was set to be 5 μL . After each measurement, the metasurface was thoroughly washed with deionized water and blow-dried with high-pressure nitrogen gas to prevent the residual glucose from causing deviation of the concentration, which may lead to inaccurate measurement of the refractive index.

2.4. Surface Functionalization and Binding

The biological mechanism of MC-LR toxicity is based on covalent binding to protein phosphatases which are key enzymes in cell regulation [5–7]. The specific binding of MC-LR (as antigen) to its antibody (mab mc10e7) is also based on this mechanism. Since MC-LR have highly reactive carboxyl groups, they can be attached to the dielectric metasurface with functionalized surfaces.

The MC-LR were attached to the metasurface broadly in four steps (Figure 1). In the first step, the metasurface was rendered hydrophilic to obtain a sufficient number of hydroxyl groups on the surface of the silicon structure. Thereafter, the hydroxyl groups were converted to amino end chains by (3-Aminopropyl) triethoxysilane (APTES). In the next step, the amino end chains were converted to carboxyl end chains by the imide reaction. Finally, the activated esters were obtained by 1-(3-Dimethylaminopropyl)-3-ethylcarbodiimide hydrochloride (EDC) and N-Hydroxysuccinimide (NHS), and they bound to the carboxyl group of the MC-LR molecules. A detailed description of these steps is provided below.

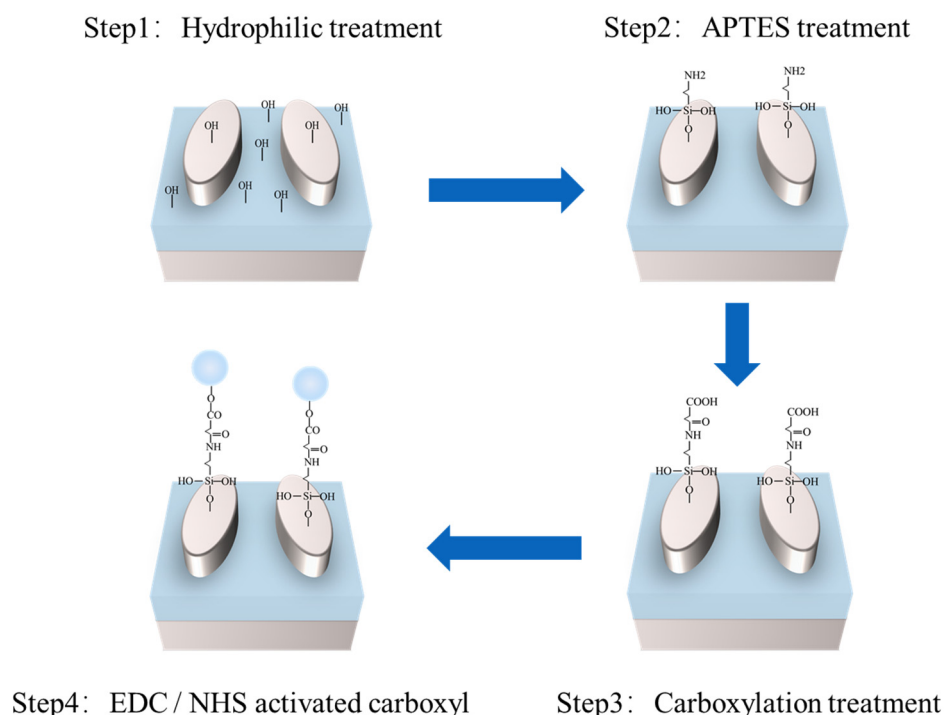


Figure 1. Schematic diagram showing the steps to attach MC-LR to the surface of a dielectric metasurface.

Hydrophilic treatment. The dielectric metasurface was immersed in a piranha solution, which is a mixture of concentrated sulfuric acid and hydrogen peroxide solution in the ratio of 3:1 by volume, and it was left for more than 3 h at room temperature. Afterwards, the metasurface was rinsed with deionized water and dried with nitrogen gas. The metasurface was stored in a beaker with deionized water to prevent the formation

of silicon-oxygen bridge bonds on the surface of the metasurfaces, which may affect the subsequent functionalization.

APTES treatment. The metasurface was removed from the beaker of deionized water and then dried with high-purity nitrogen gas. Next, it was immersed in an acetone solution containing 2% APTES by volume and left for more than 3 h at room temperature. The metasurface was washed more than twice with acetone solution, anhydrous ethanol, and deionized water in turn, and finally blow-dried with high purity nitrogen gas.

Carboxylation treatment. The dried metasurface was immersed in a saturated solution of succinic anhydride in anhydrous ethanol and left for more than 4 h (even overnight) at room temperature. Finally, the metasurface was washed multiple times (more than twice) with anhydrous ethanol and deionized water, respectively, and blow-dried with high purity nitrogen gas. It can be noted that the succinic anhydride solution should not be allowed to come in contact with water during the whole process, otherwise the succinic anhydride will hydrolyze and affect the functionalization of the structure surface.

Activated ester treatment. EDC (75 mmol/L) was dissolved in ethanol solution and NHS (25 mmol/L) was dissolved in phosphate buffer saline with pH of 7.4, and then EDC is mixed with NHS in a 3:1 volume ratio. The metasurface was immersed in the EDC/NHS mixture for 20 min at room temperature. Thereafter, the metasurface was washed with deionized water and blow-dried with high-purity nitrogen gas. Afterwards, the metasurface was placed in the incubator, and 40 μ L MC-LR solution was added to the top surface of the metasurface. Subsequently, different concentrations of MC-LR solution were added dropwise, according to the measurement requirements. The incubator was kept in a moist environment and incubated for 30 min.

Finally, the functionalization of the surface of the dielectric metasurface was completed and 40 μ L of antibody was dropped onto the functionalized metasurface and incubated for 30 min to complete the binding process.

2.5. Materials and Chemicals

The SOI substrate, the negative resist (AR-N 7520.11), and the glucose (purity \geq 99.5%) were purchased from ICEMOSTECH, AllResist, and Sigma-Aldrich, respectively. The purchasing details of the chemicals used for surface functionalization and binding process are as follows. The MC-LR and its antibody (mab mc10e7) were purchased from Beijing Puhuashi Technology Development Co. Ltd. (Beijing, China), the APTES was purchased from Beyotime, and the EDC was purchased from Bioss. Whereas the NHS, the succinic anhydride, and the phosphate buffer saline were purchased from Sigma-Aldrich, Bidepharma, and MACKLIN, respectively.

2.6. Optical Characterization

To record the transmission spectrum of the metasurface and sensing analyte, an experimental setup consisting of a transmission light system was built. A supercontinuum laser (YSL RAINBOW-1040-01) was used as a near-infrared light source with a broad range of 600–1700 nm. A pair of 20 \times Mitutoyo infrared objective lenses was fixed above and below the metasurface stage separately to focus the laser light onto the metasurface and collect the transmitted light, respectively. A fiber-optic probe fitted with a convergent lens was used to guide the signal to the spectrometer (AQ-6315A).

3. Results and Discussion

3.1. Design and Characterization

The designed dielectric metasurface consists of periodic arrays of two mirror-symmetric elliptical disc structures made of silicon with a certain deflection angle (Figure 2a). The metasurface is fabricated on the SOI substrate with a 3 μ m SiO₂ buffer layer. In FDTD simulation, the thickness of the elliptical discs is fixed at 220 nm. The long and short axes of the discs are set to be 560 nm and 240 nm, respectively. The distance between the two centers of the discs is considered to be 450 nm. The periods along the X- and

Y-directions are 900 nm and 760 nm, respectively. The deflection angle between Y-axis and the long axis of the ellipse is 10° . Under x-polarized incident light excitation, there is an obvious resonance peak at 1427 nm in the simulated transmission spectrum (Figure 2b). The linewidth of the resonance peak is about 4.5 nm and the corresponding quality factor comes out to be 317. The narrow linewidth and high-quality factor allow the dielectric metasurface to distinguish small spectral shifts and enhances its potential to be a highly sensitive detector.

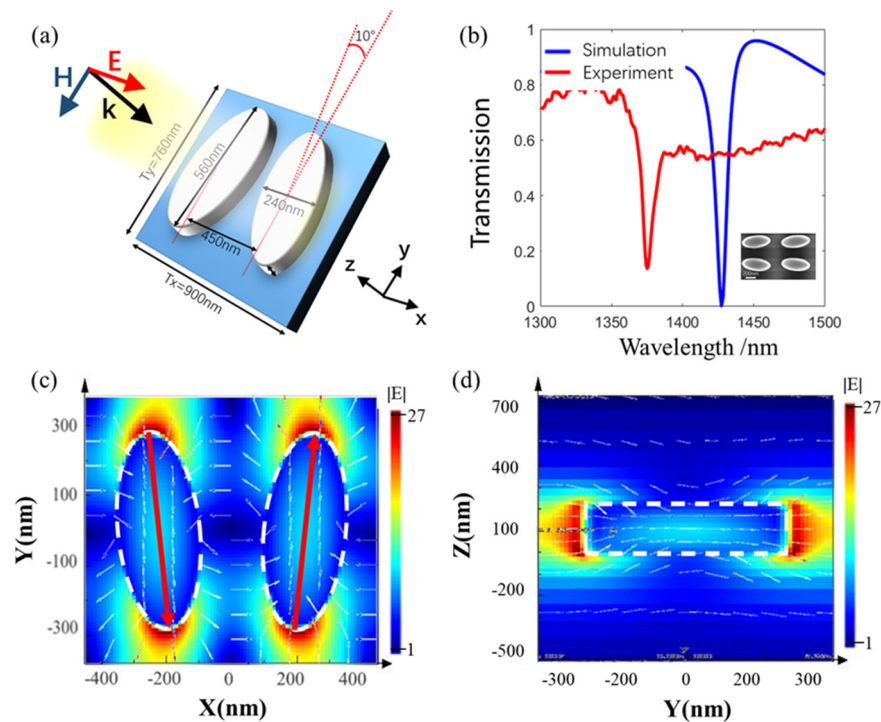


Figure 2. Design and characterization of the dielectric metasurface. (a) Diagram of the elliptical silicon disc pair. (b) Transmission spectra obtained in experiment and simulation. Inset shows a scanning electron microscope image of the fabricated metasurface. (c,d) The electric field diagram and the electric field vector diagram of the metasurface at the resonance wavelength of 1427 nm in XY-plane and YZ-plane.

The resonance at 1427 nm is an electric QBIC mode. It can be observed that the electric field concentration occurs towards the ends of the long axis of the elliptical discs (Figure 2c,d). The internal electric fields of the two discs are in opposite phases. In this way, the electromagnetic field energy concentration around the structure leads to the enhancement of local electric field intensity. As a result, it becomes sensitive to small changes in the surrounding refractive index caused by the binding of the detection analyte.

When the elliptical deflection angle is 0 degrees, the bound states in the continuum mode cannot directly get excited by the outside light field, thereby, the resonance peak does not appear on the transmission spectrum. However, when the deflection angle is increased, BIC mode changes to QBIC, which can couple with the external light field. The magnitude of radiation loss is related to the deflection angle of the ellipse. A smaller deflection angle (not 0 degrees) can support a QBIC mode with smaller radiation loss, which ensures that the resonance bandwidth is narrower and the corresponding quality factor is higher [49,50]. It is imperative to mention that the quality factor can be controlled by adjusting the deflection angle.

It is observed that a part of the electromagnetic field of the QBIC mode is outside the elliptical structure, which makes it sensitive to the change of refractive index of its immediate surrounding. The electric field corresponding to the QBIC mode shown in Figure 2c,d

can couple with the external electric field. The polarization direction of the incident light is parallel to the X-axis, and the electric field in the ellipse also has a component in the same direction, thereby, this mode can be excited by an external electric field. In this way, the QBIC mode can be coupled to free space, and it appears as a resonance peak with a certain linewidth on the transmitted spectrum.

The major and minor axes of the fabricated elliptical structure are 530 nm and 224 nm, respectively. The distance between the two centers of the discs is 451 nm. The period along the X- and Y-directions are 908 nm and 783 nm, respectively. The deflection angle is 12° . An obvious resonance peak is observed at 1375 nm in the experimental transmission spectrum (Figure 2b), and the corresponding quality factor comes out to be ~ 170 . By comparing with the simulation result, it can be concluded that the resonance peak is caused by a QBIC resonance. The deviation of the resonant peak wavelength between the experimental and simulation results can be attributed to imperfections of the fabricated metasurface, including shape deformation and scattering loss.

3.2. Sensing Measurement

A dielectric metasurface can be used for high-sensitive optical sensing, provided the linewidth of its resonance peak is narrow. The sensing principle is based on the influence of the change of the surrounding refractive index on the resonance wavelength. In order to determine the refractive index sensitivity of the metasurface in the experiment, different concentrations of glucose solutions are used to represent different refractive indices. The concentration of the glucose solution and its refractive index have an accurate correspondence [51].

In the experiment, glucose solutions with mass fractions of 10%, 20%, 30%, and 40% are dropped on the surface of the metasurface. Deionized water is used as a reference which can be regarded as a glucose solution with a concentration of 0%. The measured spectra with different concentrations at 20°C are shown in Figure 3a. It can be seen that the resonance peak in the transmission spectrum redshifts with increasing glucose concentration. It demonstrates that the QBIC resonance can be applied to environmental refractive index sensing.

The linewidth ($\Delta\lambda$) of the resonance peak and the shift of resonance wavelength per refractive-index-unit change (S) are two important evaluation indicators for the sensors based on optical resonance. A figure of merit (FOM) can be defined as $\text{FOM} = S/\Delta\lambda$ [26]. From the shift of the resonance peak wavelength with the change of the environment refractive index, the linear dependence between these two parameters can be fitted with $n = 0.0012\Delta\lambda + 1.326$ (Figure 3b). According to the fitted linear equation, the sensitivity of the dielectric metasurface is ~ 788 nm/RIU, and the FOM is ~ 99.3 . This is a clear demonstration of the fact that the dielectric metasurface can respond to small changes in the environmental refractive index, which can greatly improve the reliability and sensitivity of the detection of microscale analytes.

The dielectric metasurface can further be used for specific recognition and sensitive detection of MC-LR based on antigen and antibody binding methods. The molecular weight of MC-LR is 995.2, which is very small. Therefore, the refractive index change caused by coupling with low-concentration MC-LR is very small, and it is hard to obtain a resolvable peak shift on the spectrum. With the binding of the antibody (molecular weight is 150,000), MC-LR's antigen-antibody pair can cause greater refractive index changes at low concentrations than MC-LR itself so that a significant shift can be seen on the spectrum. Limited by the small molecular weight of MC-LR, the sensor measurement is suitable for pure MC-LR sensing.

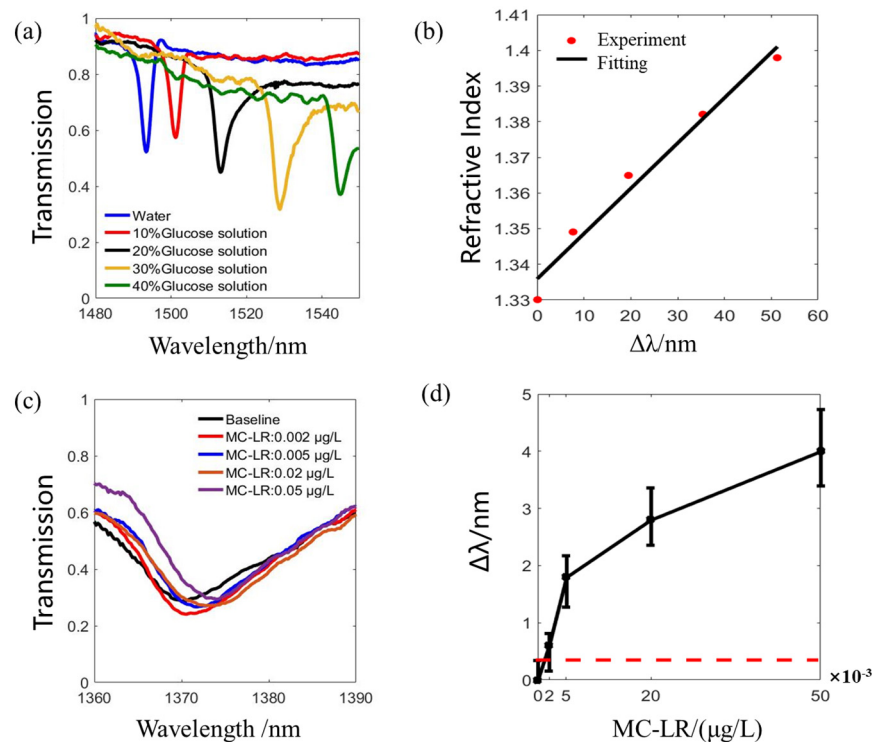


Figure 3. Refractive index sensitivity detection and MC-LR detection. (a) The transmission spectrum under different background refractive indices, where the different background refractive indices are obtained by water and different concentrations of glucose solutions. (b) The relationship between the environmental refractive index and the offset of the resonant wavelength. (c) Transmission spectrum with different MC-LR concentrations. (d) The relationship between the MC-LR concentrations and the offset of the resonant wavelength. The red dotted line marks the wavelength shift caused by the environment.

In the experiment, four concentrations (0.002 $\mu\text{g/L}$, 0.005 $\mu\text{g/L}$, 0.02 $\mu\text{g/L}$, and 0.05 $\mu\text{g/L}$) of MC-LR are used as the analytes to be detected. As the concentration increases, more MC-LR antibody molecules get attached to the metasurface, leading to an increase in the environmental refractive index and the resonance peak wavelength redshifts in the transmission spectrum (Figure 3c,d). The minimum MC-LR concentration of 0.002 $\mu\text{g/L}$ results in an average shift of the resonance peak of 0.6 nm. Therefore, the sensitivity of the all-dielectric metasurface for detecting MC-LR is much higher than that of the SPR biosensor [21].

The detection limit shows that the dielectric metasurface with high-quality factor can serve as a sensing platform with high sensitivity. It is possible for the metasurface to sense the other variants of microcystin besides MC-LR. Because they all have the carboxyl group [5,52], the other variant of microcystin can also be coupled to the metasurface, and they can be detected with their corresponding antibodies.

4. Conclusions

This article demonstrates an all-dielectric metasurface for sensing MC-LR experimentally with high-quality factor and high sensitivity. First, the all-dielectric device provides a harmless, feasible, and stable detection platform for precise biological monitoring. As the dielectric has no thermal effect, the dielectric metasurface does not damage living tissues for in vivo sensing. Second, the high sensitivity enables it to promptly warn about the presence of MC-LR pollution in freshwater bodies to prevent catastrophic harm to human and animal lives. Third, the dielectric metasurface can also be combined with microfluidics to realize real-time dynamic monitoring of biologically active molecules. Finally, the dielec-

tric metasurface can be fabricated on flexible material and used in smart wearable devices to achieve real-time health monitoring. Essentially, the dielectric metasurface provides a highly sensitive sensing platform for MC-LR and can be extended to other target analytes, such as viruses.

Author Contributions: Conceptualization, B.M., A.O. and Q.L.; methodology, B.M. and A.O.; software, A.O.; validation, B.M. and A.O.; formal analysis, B.M.; investigation, B.M.; data curation, B.M.; writing—original draft preparation, B.M., A.O. and J.Z.; writing—review and editing, B.M., P.G. and Q.L.; supervision, Q.L.; project administration, P.A.B., R.K.S., W.Q. and Q.L.; funding acquisition, Q.L. All authors have read and agreed to the published version of the manuscript.

Funding: This research was funded by the National Key Research and Development Program of China, grant number 2017YFE0100200, the National Natural Science Foundation of China, grant number 61775194 and 61950410608, the Open Foundation of the State Key Laboratory of Modern Optical Instrumentation and Zhejiang University K.P.Chao's High Technology Development Foundation.

Data Availability Statement: The data presented in this study are available within the article.

Acknowledgments: The authors would like to acknowledge the ZJU Micro-Nano Fabrication Center for the access of EBL and Tianjin H-Chip Technology Group Corporation for the support of ICP-RIE.

Conflicts of Interest: The authors declare no conflict of interest.

Abbreviations

The following abbreviations are used in this manuscript:

MC-LR	Microcystin-LR
QBIC	Quasi bound states in the continuum
SPR	Surface plasmon resonances
RIU	Refractive index unit
FDTD	Finite-Difference Time-Domain
SOI	Silicon on insulator
APTES	(3-Aminopropyl) triethoxysilane
EDC	1-(3-Dimethylaminopropyl)-3-ethylcarbodiimide hydrochloride
NHS	N-Hydroxysuccinimide
FOM	Figure of merit

References

- van Apeldoorn, M.E.; van Egmond, H.P.; Speijers, G.J.A.; Bakker, G.J.I. Toxins of cyanobacteria. *Mol. Nutr. Food Res.* **2007**, *51*, 7–60. [[CrossRef](#)] [[PubMed](#)]
- Humbert, J.F. Toxins of cyanobacteria. In *Handbook of Toxicology of Chemical Warfare Agents*; Elsevier Inc.: Amsterdam, The Netherlands, 2009; pp. 371–379.
- Mantzouki, E.; Lüring, M.; Fastner, J.; de Senerpont Domis, L.; Wilk-Woźniak, E.; Koreivienė, J.; Seelen, L.; Teurlinx, S.; Verstijnen, Y.; Krztoń, W.; et al. Temperature effects explain continental scale distribution of cyanobacterial toxins. *Toxins* **2018**, *10*, 156. [[CrossRef](#)]
- Zhang, C.; Massey, I.Y.; Liu, Y.; Huang, F.; Gao, R.; Ding, M.; Xiang, L.; He, C.; Wei, J.; Li, Y.; et al. Identification and characterization of a novel indigenous algicidal bacterium *Chryseobacterium* species against *Microcystis aeruginosa*. *J. Toxicol. Environ. Health Part A* **2019**, *82*, 845–853. [[CrossRef](#)]
- Massey, I.Y.; Yang, F.; Ding, Z.; Yang, S.; Guo, J.; Tezi, C.; Al-Osman, M.; Kamegni, R.B.; Zeng, W. Exposure routes and health effects of microcystins on animals and humans: A mini-review. *Toxicon* **2018**, *151*, 156–162. [[CrossRef](#)]
- Alosman, M.; Cao, L.; Massey, I.Y.; Yang, F. The lethal effects and determinants of microcystin-LR on heart: A mini review. *Toxin Rev.* **2020**, 1–10. [[CrossRef](#)]
- An, J.S.; Carmichael, W.W. Use of a colorimetric protein phosphatase inhibition assay and enzyme linked immunosorbent assay for the study of microcystins and nodularins. *Toxicon* **1994**, *32*, 1495–1507. [[CrossRef](#)]
- Zhang, S.; Liu, C.; Li, Y.; Imam, M.U.; Huang, H.; Liu, H.; Xin, Y.; Zhang, H. Novel role of ER stress and autophagy in microcystin-LR induced apoptosis in chinese hamster ovary cells. *Front. Physiol.* **2016**, *7*, 527. [[CrossRef](#)]
- McLellan, N.L.; Manderville, R.A. Toxic mechanisms of microcystins in mammals. *Toxicol. Res.* **2017**, *6*, 391–405. [[CrossRef](#)] [[PubMed](#)]
- Yang, S.; Chen, L.; Wen, C.; Zhang, X.; Feng, X.; Yang, F. MicroRNA expression profiling involved in MC-LR-induced hepatotoxicity using high-throughput sequencing analysis. *J. Toxicol. Environ. Health Part A* **2018**, *81*, 89–97. [[CrossRef](#)] [[PubMed](#)]

11. Wharton, R.E.; Cunningham, B.R.; Schaefer, A.M.; Guldborg, S.M.; Hamelin, E.I.; Johnson, R.C. Measurement of microcystin and nodularin activity in human urine by immunocapture-protein phosphatase 2a assay. *Toxins* **2019**, *11*, 729. [[CrossRef](#)]
12. Chen, L.; Yang, S.; Wen, C.; Zheng, S.; Yang, Y.; Feng, X.; Chen, J.; Luo, D.; Liu, R.; Yang, F. Regulation of microcystin-LR-induced DNA damage by miR-451a in HL7702 cells. *Toxins* **2019**, *11*, 164. [[CrossRef](#)] [[PubMed](#)]
13. Sanz Lobón, G.; Yepez, A.; Garcia, L.F.; Morais, R.L.; Vaz, B.G.; Carvalho, V.V.; De Oliveira, G.A.R.; Luque, R.; Gil, E.D.S. Efficient electrochemical remediation of microcystin-LR in tap water using designer TiO₂@carbon electrodes. *Sci. Rep.* **2017**, *7*, 41326. [[CrossRef](#)] [[PubMed](#)]
14. World Health Organization. Cyanobacterial toxins: Microcystin-LR in drinking-water. In *Guidelines for Drinking-Water Quality*, 2nd ed.; World Health Organization: Geneva, Switzerland, 1998; pp. 1–14.
15. Catanante, G.; Espin, L.; Marty, J.L. Sensitive biosensor based on recombinant PP1 α for microcystin detection. *Biosens. Bioelectron.* **2015**, *67*, 700–707. [[CrossRef](#)] [[PubMed](#)]
16. Parker, C.H.; Stutts, W.L.; Degrasse, S.L. Development and Validation of a Liquid Chromatography-Tandem Mass Spectrometry Method for the Quantitation of Microcystins in Blue-Green Algal Dietary Supplements. *J. Agric. Food Chem.* **2015**, *63*. [[CrossRef](#)]
17. Marsan, D.W.; Conrad, S.M.; Stutts, W.L.; Parker, C.H.; Deeds, J.R. Evaluation of microcystin contamination in blue-green algal dietary supplements using a protein phosphatase inhibition-based test kit. *Heliyon* **2018**, *4*, e00573. [[CrossRef](#)]
18. Wharton, R.E.; Ojeda-Torres, G.; Cunningham, B.; Feyereisen, M.C.; Hill, K.L.; Abbott, N.L.; Seymour, C.; Hill, D.; Lang, J.; Hamelin, E.I.; et al. Quantification of Microcystin-LR in Human Urine by Immunocapture Liquid Chromatography Tandem Mass Spectrometry. *Chem. Res. Toxicol.* **2018**, *31*, 898–903. [[CrossRef](#)]
19. Yuan, J.; Kim, H.J.; Filstrup, C.T.; Guo, B.; Imerman, P.; Ensley, S.; Yoon, K.J. Utility of a PCR-based method for rapid and specific detection of toxigenic *Microcystis* spp. in farm ponds. *J. Vet. Diagn. Investig.* **2020**, *32*, 369–381. [[CrossRef](#)]
20. Hu, C.; Gan, N.; Chen, Y.; Bi, L.; Zhang, X.; Song, L. Detection of microcystins in environmental samples using surface plasmon resonance biosensor. *Talanta* **2009**, *80*, 407–410. [[CrossRef](#)]
21. Herranz, S.; Bocková, M.; Marazuela, M.D.; Homola, J.; Moreno-Bondi, M.C. An SPR biosensor for the detection of microcystins in drinking water. *Anal. Bioanal. Chem.* **2010**, *398*, 2625–2634. [[CrossRef](#)]
22. Vinogradova, T.; Danaher, M.; Baxter, A.; Moloney, M.; Victory, D.; Haughey, S.A. Rapid surface plasmon resonance immunobiosensor assay for microcystin toxins in blue-green algae food supplements. *Talanta* **2011**, *84*, 638–643. [[CrossRef](#)]
23. Sun, S.; He, Q.; Hao, J.; Xiao, S.; Zhou, L. Electromagnetic metasurfaces: Physics and applications. *Adv. Opt. Photonics* **2019**, *11*, 380. [[CrossRef](#)]
24. Grupp, W. Optical performance monitoring in optical transport networks. In *Optical Performance Monitoring*; Elsevier Inc.: Amsterdam, The Netherlands, 2010; pp. 385–421.
25. Yang, Y.; Kravchenko, I.I.; Briggs, D.P.; Valentine, J. All-dielectric metasurface analogue of electromagnetically induced transparency. *Nat. Commun.* **2014**, *5*, 1–7. [[CrossRef](#)] [[PubMed](#)]
26. Zijlstra, P.; Paulo, P.M.R.; Orrit, M. Optical detection of single non-absorbing molecules using the surface plasmon resonance of a gold nanorod. *Nat. Nanotechnol.* **2012**, *7*, 379–382. [[CrossRef](#)]
27. Mahmoudi, M.; Lohse, S.E.; Murphy, C.J.; Fathizadeh, A.; Montazeri, A.; Suslick, K.S. Variation of protein corona composition of gold nanoparticles following plasmonic heating. *Nano Lett.* **2014**, *14*, 6–12. [[CrossRef](#)] [[PubMed](#)]
28. Luo, H.; Li, Q.; Du, K.; Xu, Z.; Zhu, H.; Liu, D.; Cai, L.; Ghosh, P.; Qiu, M. An ultra-thin colored textile with simultaneous solar and passive heating abilities. *Nano Energy* **2019**, *65*, 103998. [[CrossRef](#)]
29. Luo, H.; Zhu, Y.; Xu, Z.; Hong, Y.; Ghosh, P.; Kaur, S.; Wu, M.; Yang, C.; Qiu, M.; Li, Q. Outdoor Personal Thermal Management with Simultaneous Electricity Generation. *Nano Lett.* **2021**, *21*, 3879–3886. [[CrossRef](#)]
30. Bontempi, N.; Chong, K.E.; Orton, H.W.; Staude, I.; Choi, D.Y.; Alessandri, I.; Kivshar, Y.S.; Neshev, D.N. Highly sensitive biosensors based on all-dielectric nanoresonators. *Nanoscale* **2017**, *9*, 4972–4980. [[CrossRef](#)] [[PubMed](#)]
31. Mie, G. Beiträge zur Optik trüber Medien, speziell kolloidaler Metallösungen. *Ann. Phys.* **1908**, *330*, 377–445. [[CrossRef](#)]
32. Ginn, J.C.; Brener, I.; Peters, D.W.; Wendt, J.R.; Stevens, J.O.; Hines, P.F.; Basilio, L.I.; Warne, L.K.; Ihlefeld, J.; Clem, P.G.; et al. Realizing optical magnetism from dielectric metamaterials. *Phys. Rev. Lett.* **2012**, *108*, 097402. [[CrossRef](#)]
33. Caldarola, M.; Albella, P.; Cortés, E.; Rahmani, M.; Roschuk, T.; Grinblat, G.; Oulton, R.F.; Bragas, A.V.; Maier, S.A. Non-plasmonic nanoantennas for surface enhanced spectroscopies with ultra-low heat conversion. *Nat. Commun.* **2015**, *6*, 1–8. [[CrossRef](#)]
34. Decker, M.; Staude, I.; Falkner, M.; Dominguez, J.; Neshev, D.N.; Brener, I.; Pertsch, T.; Kivshar, Y.S. High-Efficiency Dielectric Huygens' Surfaces. *Adv. Opt. Mater.* **2015**, *3*, 813–820. [[CrossRef](#)]
35. Yavas, O.; Svedendahl, M.; Quidant, R. Unravelling the Role of Electric and Magnetic Dipoles in Biosensing with Si Nanoresonators. *ACS Nano* **2019**, *13*, 4582–4588. [[CrossRef](#)]
36. Decker, M.; Staude, I. Resonant dielectric nanostructures: A low-loss platform for functional nanophotonics. *J. Opt.* **2016**, *18*, 103001. [[CrossRef](#)]
37. Yang, Y.; Wang, W.; Boulesbaa, A.; Kravchenko, I.I.; Briggs, D.P.; Poretzky, A.; Geohegan, D.; Valentine, J. Nonlinear Fano-Resonant Dielectric Metasurfaces. *Nano Lett.* **2015**, *15*, 7388–7393. [[CrossRef](#)]
38. Jahani, S.; Jacob, Z. All-dielectric metamaterials. *Nat. Nanotechnol.* **2016**, *11*, 23–36. [[CrossRef](#)]
39. Proust, J.; Bedu, F.; Gallas, B.; Ozerov, I.; Bonod, N. All-Dielectric Colored Metasurfaces with Silicon Mie Resonators. *ACS Nano* **2016**, *10*, 7761–7767. [[CrossRef](#)]

40. Kruk, S.; Kivshar, Y. Functional Meta-Optics and Nanophotonics Govern by Mie Resonances. *ACS Photonics* **2017**, *4*, 2638–2649. [[CrossRef](#)]
41. Baranov, D.G.; Zuev, D.A.; Lepeshov, S.I.; Kotov, O.V.; Krasnok, A.E.; Evlyukhin, A.B.; Chichkov, B.N. All-dielectric nanophotonics: The quest for better materials and fabrication techniques. *Optica* **2017**, *4*, 814. [[CrossRef](#)]
42. Yuan, S.; Qiu, X.; Cui, C.; Zhu, L.; Wang, Y.; Li, Y.; Song, J.; Huang, Q.; Xia, J. Strong Photoluminescence Enhancement in All-Dielectric Fano Metasurface with High Quality Factor. *ACS Nano* **2017**, *11*, 10704–10711. [[CrossRef](#)] [[PubMed](#)]
43. Overvig, A.C.; Shrestha, S.; Malek, S.C.; Lu, M.; Stein, A.; Zheng, C.; Yu, N. Dielectric metasurfaces for complete and independent control of the optical amplitude and phase. *Light Sci. Appl.* **2019**, *8*, 92. [[CrossRef](#)]
44. Leitis, A.; Heßler, A.; Wahl, S.; Wuttig, M.; Taubner, T.; Tittel, A.; Altug, H. All-Dielectric Programmable Huygens' Metasurfaces. *Adv. Funct. Mater.* **2020**, *30*, 1910259. [[CrossRef](#)]
45. Ni, Y.; Chen, S.; Wang, Y.; Tan, Q.; Xiao, S.; Yang, Y. Metasurface for Structured Light Projection over 120° Field of View. *Nano Lett.* **2020**, *20*, 6719–6724. [[CrossRef](#)] [[PubMed](#)]
46. Tian, J.; Li, Q.; Belov, P.A.; Sinha, R.K.; Qian, W.; Qiu, M. High-Q All-Dielectric Metasurface: Super and Suppressed Optical Absorption. *ACS Photonics* **2020**, *7*, 1436–1443. [[CrossRef](#)]
47. Koshelev, K.; Kivshar, Y. Dielectric Resonant Metaphotonics. *ACS Photonics* **2021**, *8*, 102–112. [[CrossRef](#)]
48. Forouhi, A.R.; Bloomer, I. Calculation of Optical Constants, n and k, in the Interband Region. In *Handbook of Optical Constants of Solids*; Elsevier: Amsterdam, The Netherlands, 1998; pp. 151–175.
49. Tittel, A.; Leitis, A.; Liu, M.; Yesilkoy, F.; Choi, D.Y.; Neshev, D.N.; Kivshar, Y.S.; Altug, H. Imaging-based molecular barcoding with pixelated dielectric metasurfaces. *Science* **2018**, *360*, 1105–1109. [[CrossRef](#)]
50. Leitis, A.; Tittel, A.; Liu, M.; Lee, B.H.; Gu, M.B.; Kivshar, Y.S.; Altug, H. Angle-multiplexed all-dielectric metasurfaces for broadband molecular fingerprint retrieval. *Sci. Adv.* **2019**, *5*, eaaw2871. [[CrossRef](#)]
51. Zheyi, S.; Guoying, F.; Tao, Z. Accurate Measurement of the Refractive Index D-Glucose Solution at Various Concentrations at Different Temperatures. *Chin. J. Lasers* **2014**, *41*, 1208008. [[CrossRef](#)]
52. Zhang, H.; Gonzales, G.B.; Beloglazova, N.V.; De Saeger, S.; Shen, J.; Zhang, S.; Yang, S.; Wang, Z. Development of a validated direct injection-liquid chromatographic tandem mass spectrometric method under negative electrospray ionization for quantitation of nine microcystins and nodularin-R in lake water. *J. Chromatogr. A* **2020**, *1609*, 460432. [[CrossRef](#)]